This is to certify that the
thesis entitled

A STOCHASTIC ESTIMATION TECHNIQUE FOR
DECOMPOSITION OF IN-CYLINDER FLOWFIELDS

presented by

ANDREW ALAN SASAK

has been accepted towards fulfillment
of the requirements for the

M. S. degree in Mechanical Engineering

Major Professor's Signature

10/31/03

Date

# A STOCHASTIC ESTIMATION TECHNIQUE FOR DECOMPOSITION OF IN-CYLINDER FLOWFIELDS

By

Andrew Alan Sasak

A THESIS

Submitted to
Michigan State University
in partial fulfillment of the requirements
for the degree of

MASTER OF SCIENCE

Department of Mechanical Engineering

2003

ABSTRACT

A STOCHASTIC ESTIMATION TECHNIQUE FOR DECOMPOSITION OF IN-CYLINDER FLOWFIELDS

By

Andrew Alan Sasak

Turbulence and cycle-to-cycle variation are features of the air motion in the cylinders of all internal combustion engines. While turbulence is generally beneficial to engine performance and efficiency, cycle-to-cycle variation is undesirable. Turbulence causes better air/fuel mixing, higher flame speeds, as well as faster and more complete combustion. Cycle-to-cycle variation, on the other hand, lowers an engine's efficiency by requiring it to be tuned for the average of many different combustion processes, on account of the variability in initial conditions for the combustion event. An accurate way to predict and better understand in-cylinder fluid flow could aid in its control and in designing more efficient IC engines. For these reasons the ability to measure turbulence and cycle-to-cycle variation is an interesting subject to any engine designer.

In this study, a new stochastic estimation method was implemented to decompose a two-dimensional flowfield into its turbulent, cyclic, and mean components. This method was then applied to data acquired, using Molecular Tagging Velocimetry, in two previous studies, in which active flow control was used in an attempt to decrease cycle-to-cycle variation. The resulting decompositions, which estimate the true turbulent and cyclic variation velocity fields, provide interesting and useful data. It indicates that when acoustic excitation reduced the kinetic energy in fluctuating components of the flow, it did so by roughly the same amount in fine-scale turbulent and large scale fluctuating/cycle-to-cycle motions.

For Kristy, the love of my life

# Acknowledgements

I would like to thank Dr. Giles Brereton for his guidance throughout my college education. Dr. Ahmed Naguib and Dr. Harold Schock for their helpful criticism and suggestions. My research would not have been possible without Alvin Goh and Andy Fedewa who provided all of the data to which this method was applied and answered countless questions. I would also like to thank Tom Stuecken, Ed Timm, Yuan Shen, Mark Novak, Kyle Judd, Jan Chappell, Rob Draper, and Boon-Keat Chui who have all supported or assisted me in some way. I owe much to my parents who have given me and done for me over the years so much more than I can list, including: their love, guidance, and of course raising me. Also, my sister, Angela, for being my sister and making me laugh. I am grateful for the love and support I have received from my girlfriend's family. I thank my grandparents for everything they have taught me, and my Godparents Tom and Sandy Pitsch for their part in my decision to pursue an education in Mechanical Engineering. Kristy, thank you for all of your love and motivation; I could not have finished this without you. Finally, I would like to thank God, for the gifts and blessings He has given me.

# Contents

# List of Tables

# List of Figures

# Chapter 1

# Introduction

## 1.1 Motivation

This thesis is concerned with the understanding of velocity fields in engine cylinders. There are numerous reasons for trying to improve the understanding and accuracy of predictions of velocity fields in IC engine cylinders. First, such flows are turbulent and therefore cannot be described in averaged form exactly. Second, turbulence has several qualities relating to combustion. Increased turbulence can result in better air/fuel mixing. At ignition, high levels of turbulence can lead to higher flame speeds, as well as more rapid and complete combustion. These effects are all desired by engine designers. Conversely these higher turbulence levels also increase the rate of heat transfer to the cylinder walls, which can reduce the thermal efficiency of the process. Another interesting aspect of in-cylinder flow is cycle-to-cycle variation: the organized variation of air and fuel flow from one engine cycle to the next. Figure 1.1 demonstrates cycle-to-cycle variation in the in-cylinder velocity fields of two consecutive engine cycle. Cycle-to-cycle variation is undesirable because it causes inconsistency in the initial conditions of the combustion event and prevents engines from being tuned optimally. It can also cause misfire in lean-burn engines and therefore limits their range of operation. If cycle-to-cycle variation could be measured, understood, and controlled, engine performance might be improved significantly.

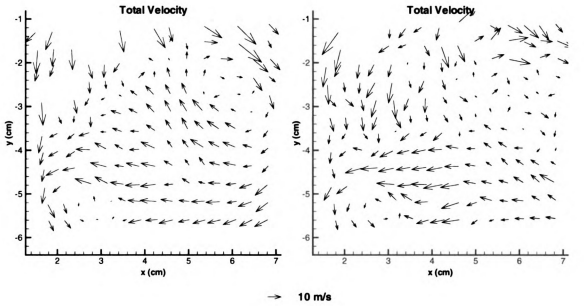


Figure 1.1: Consecutive cycles from Ford 4.6 L engine at 90 CAD, 600 rpm demonstrating cycle-to-cycle variation

## 1.2 The problem of decomposing unsteady turbulent flows

Presently, several techniques exist which may be used to measure in-cylinder velocity fields in research engines. Dividing these velocity fields into their turbulent and non-turbulent components is straightforward for statistically stationary flows, using the Reynolds decomposition. In such a flow, the non-turbulent component is the mean velocity, and the turbulent one is the remainder of the flowfield (difference between the instantaneous flowfield and the mean velocity flowfield) by definition. However, engine flows are not at all stationary and there are significant cycle-to-cycle variations in velocity that are not turbulent. If the Reynolds decomposition technique is used for these engine flows, then these cycle-to-cycle variations are incorrectly considered to be parts of the turbulent components. In order to better understand in-cylinder turbulent flow, it is desirable to have some technique to separate the cyclic variation from the turbulent flowfield.

## 1.3 Previous work

Although cycle-to-cycle variation is a subject of long-standing interest to automotive researchers, relatively little work has been done to quantify it. Hall and Bracco [1] used a cycle-resolved analysis of LDV measurements to separate turbulence from low frequency bulk flow. Since the bulk flow was determined in each cycle, they were also able to determine how much the bulk velocity varied from one cycle to another (the cycle-to-cycle variation). They noted that the magnitude of cyclic variation was at least as large as the turbulent intensity in their study, demonstrating the significant degree of cyclic variation in in-cylinder flow. Additionally, Brereton and Kodal [2] have demonstrated a method using data-adaptive turbulence filters to procure the turbulent component of a flow. Using this method the turbulence filter will find the turbulent component to be the portion of the flow with a spectral shape resembling that expected of a stationary turbulent flow. Since the turbulent component can be separated, the cyclic variation is the difference between the mean and the non-turbulent part.

In this work, stochastic estimation of decomposed velocity fields is investigated. The stochastic estimation technique was first proposed to obtain an estimate of conditional averages by Adrian [3]. Over the past twenty seven years many papers have been published on the subject of using stochastic estimation to approximate conditional averages [4, 5]. The method used in this paper to decompose non-stationary, non-ergodic turbulent flow data, which uses stochastic estimation, was developed by Brereton [6]. All these methods require some kind of assumption to be made about either the turbulent field or the cycle-to-cycle variation. Since no general assumption can be uniformly valid for either all turbulent flows or all cyclic variations in the velocity, the best one can do is make an assumption that seems reasonable and estimate the turbulent and cycle-to-cycle fields accordingly. In this thesis, a stochastic estimation is made of each velocity field and applied to experimental measurements

of velocity in planes through the combustion chamber of research engines. The experimental measurements and decomposition technique are described in the following chapters.

# Chapter 2

# Experimental Apparatus

## 2.1 Molecular Tagging Velocimetry experimental setup

The fields of velocities measured in engine cylinders, and used for this study were from two different sources. The first was provided by Goh and the second by Fedewa, who each obtained the data using a velocity measurement technique called Molecular Tagging Velocimetry (MTV) during the course of their own research. The purpose of these two previous studies was to investigate the effects of acoustic excitation on in-cylinder flow. The technique called MTV was originally pioneered by Falco and Hilbert under the name laser induced phosphorescent anemometry (LIPA). It was subsequently refined, developed and extended from liquid to gas flows, by Koochesfahani, as molecular tagging velocimetry (MTV). Koochesfahani and coworkers effectively advanced the technique from a promising research idea to a validated measurement tool, which is now being used for routine measurements of in-cylinder flows at MSU's Engine Research Laboratory. This method uses a tracer molecule such as biacetyl, which phosphoresces for a short period of time after being excited. This tracer molecule is introduced to nitrogen gas flowing in the field of interest. (Nitrogen is used in place of air since oxygen quenches the phosphorescence of the biacetyl.) Intersecting pulsed-laser lines illuminate the field of interest, forming a grid, and excite, or "tag", the biacetyl. An image is recorded at the instant of the laser pulse and another image

is recorded after a specified delay, while the biacetyl is still phosphorescing. This process of introducing laser excitation and recording images is synchronized with a particular crank angle degree, and repeated for a specified number of cycles. The MTV software computes a grid of velocity vectors by measuring the displacement of each grid intersection from the undelayed image (Figure 2.1) to the delayed image (Figure 2.2). This calculation is done for each cycle, resulting in a data file containing a series of instantaneous velocity vectors measured in the plane of the laser grids.

Molecular tagging velocimetry was used by both Goh and Fedewa to obtain flow-field data from optically accessible motored engines. For his study, Goh used a Ford cylinder head from a 4-valve 4.6 L V8 prototype engine. This head was used in concert with an optically accessible quartz cylinder and a single cylinder research engine block. An optically accessible flat-head piston was used in the research engine. The research engine was powered by a 10 HP electrical motor. The engine specifications for this setup are shown in Table 2.1.

Table 2.1: Ford 4.6 L engine specifications.

| | |
|---|---|
| Bore | 90.2 mm |
| Stroke | 90.0 mm |
| Connecting rod length | 150.7 mm |
| Valve activation | DOHC |
| Intake valve diameter | 37.0 mm |
| Exhaust valve diameter | 30.0 mm |
| Maximum valve lift | 10.02 mm at 120 CAD |
| Zero CAD | Intake TDC |
| Intake valve opening | 6 CAD before TDC |
| Intake valve closure | 250 CAD after TDC |
| Exhaust valve opening | 126 CAD after TDC |
| Exhaust valve closure | 16 CAD after TDC |
| Compression ratio | 9.85 : 1 |
| Piston top | Flat |
| Head | Bowled |

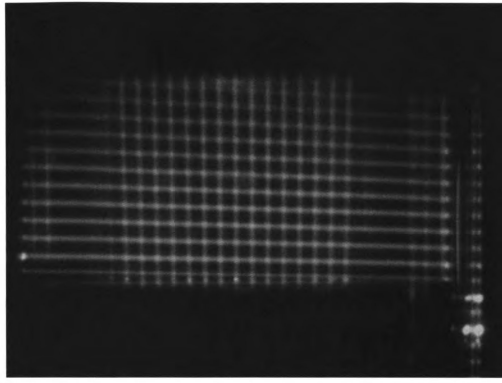

Figure 2.1: Example of an undelayed planar MTV image

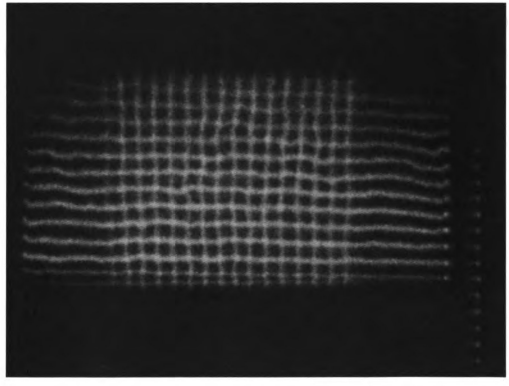

Figure 2.2: Example of a delayed planar MTV image

A Hatz 1D81Z single cylinder diesel engine was used by Fedewa to be the base for his optical engine. The cylinder head, which was designed at Michigan State University, had four valves, a combustion chamber with a flat top, and a centrally located spark plug. To make this engine optically accessible, a quartz cylinder was attached above the standard Hatz engine cylinder. A piston extension was also mounted to the top of the Hatz piston, with a second, identical piston attached to the top of the extension. The engine was rebalanced due to the increase of reciprocating mass. The engine specifications for this setup are shown in Table 2.2.

Goh created a nearly orthogonal laser grid pattern by intersecting laser beams entering the cylinder from the bottom through a quartz window in the piston with other beams entering horizontally through the quartz cylinder. This laser beam configuration is shown in Figure 2.3. This setup caused problems for the study by Fedewa. The design of the intake manifold used by Fedewa caused the evaporated biacetyl to condense and eventually create a film on the top of the piston. This film would cause the incoming laser lines to diverge and become less distinct. To circumvent this problem, a modified laser grid pattern was designed. This laser beam configuration is shown in Figure 2.4. Instead of the quasi-orthogonal grid pattern used by Goh, both laser beams entered through the cylinder wall from opposite sides, each at an angle of 30 degrees above horizontal.

Table 2.2: MSU flat-head engine specifications.

| | |
|---|---|
| Bore | 79.5 mm |
| Stroke | 100 mm |
| Connecting Rod Length | 151 mm |
| Intake Valve Diameter | 25.4 mm |
| Exhaust Valve Diameter | 25.4 mm |
| Zero CAD | Intake TDC |
| Compression ratio | 9 : 1 |
| Piston Top | Flat |
| Head | Flat |

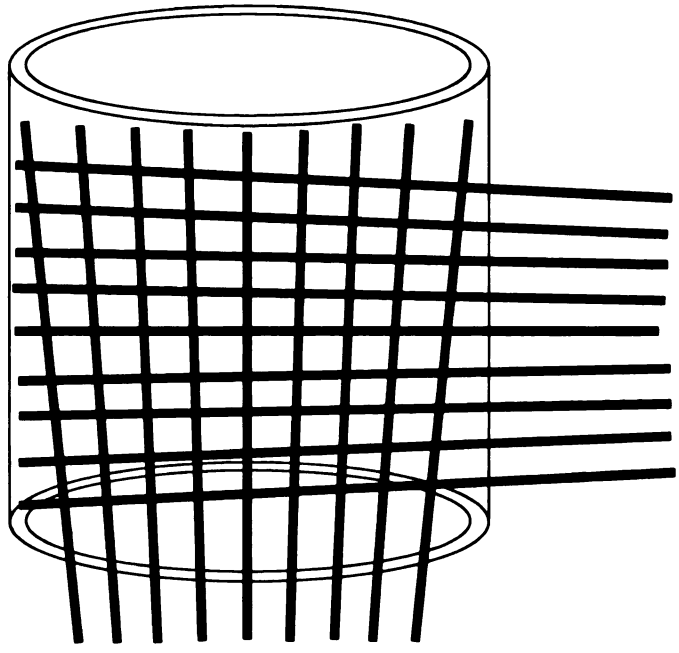

Figure 2.3: Goh laser beam configuration

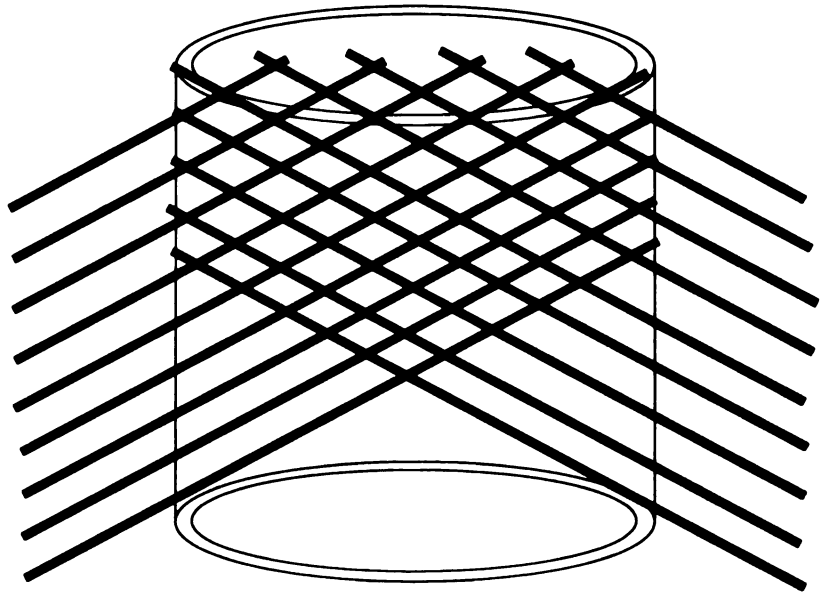

Figure 2.4: Fedewa laser beam configuration

For his study, Goh obtained velocity data at 90, 180, and 270 CAD with excitation frequencies ranging from 50 Hz to 1000 Hz. Fedewa estimated that excitation would be most effective at approximately 1800 Hz. His study therefore tested frequencies ranging from 1500 Hz to 2500 Hz in 100 Hz increments. Fedewa obtained reference velocity data at 90, 180, and 270 CAD without excitation, and tested excitation at only 270 CAD.

The vector fields of instantaneous velocities from these two studies were used as the sample data on which stochastic estimations of the turbulent and cyclic-variation components of velocity were then estimated. The decomposition procedure is described in the following chapter.

# Chapter 3

# Decomposition by Stochastic Estimation

## 3.1 Theory of stochastic estimation of spatially correlated and uncorrelated velocity components

A stationary flowfield of velocity, $u(x,t)$, can be decomposed into the sum of the ensemble average, $\langle u(x,t)\rangle$, and the deviation from that average, $u'(x,t)$, where the ensemble average is, by definition, the average over multiple, repeated, independent events, so:

$$u(x,t) = \langle u(x,t)\rangle + u'(x,t) \tag{3.1}$$

To account for the cyclic variation which is inherent to non-stationary in-cylinder fluid flow, an additional component, $\tilde{u}$, that describes organized, non-turbulent deviations from the mean is added to the standard decomposition, such that:

$$u = \langle u\rangle + \tilde{u} + u' \tag{3.2}$$

where

$\langle u\rangle$: ensemble average

$\tilde{u}$: cycle-to-cycle variation

$u'$: fluctuating component

Experimentally we can measure $u$ and compute $\langle u \rangle$ from multiple ensembles of $u$, and so Equation 3.2 can be rewritten as $u - \langle u \rangle = \tilde{u} + u'$. In order to successfully separate the cycle-to-cycle variation from the fluctuating component, some assumption must be made. However, it is known empirically that the time and space correlations of turbulent variables become zero when the correlation distance is sufficiently large. Therefore, for a sufficiently large $\Delta x$,

$$\langle (\tilde{u} + u')_x (\tilde{u} + u')_{x+\Delta x} \rangle \longrightarrow \langle \tilde{u}_x \tilde{u}_{x+\Delta x} \rangle \tag{3.3}$$

This is true if the cross-correlation between $\tilde{u}$ and $u'$ is negligible, which we assume is the case. This two-point-correlation information can be used to construct stochastic estimates of $\tilde{u}(x,t)$ and $u'(x,t)$ (which will be denoted $\tilde{u}_E(x,t)$ and $u'_E(x,t)$), given the measured value of $\tilde{u} + u'$ at location $x + \Delta x$. The stochastic estimate would seek to minimize the squares of the errors between $\tilde{u}_E$ and $\tilde{u}$ and between $u'_E$ and $u'$. This estimate would be subject to the side condition that $\tilde{u}_E(x) + u'_E(x) = \tilde{u}(x) + u'(x)$. The method of Lagrange multipliers is used, and the Lagrangian is set to:

$$\begin{aligned} \mathscr{L} = [\tilde{u}(x) - A - B(\tilde{u} + u')_{x+\Delta x}]^2 + [u'(x) - A - B(\tilde{u} + u')_{x+\Delta x}]^2 \\ + \lambda[\tilde{u}_E(x) + u'_E(x) - \tilde{u}(x) - u'(x)] \end{aligned} \tag{3.4}$$

The following partial derivatives of $L$ are set to zero.

$$\begin{aligned} \frac{\partial \mathscr{L}}{\partial A} &= -2u'(x) + 2A + \lambda = 0 \\ \frac{\partial \mathscr{L}}{\partial B} &= -2u'(x)(u' + \tilde{u})_{x+\Delta x} + 2B(u' + \tilde{u})^2_{x+\Delta x} + \lambda(u' + \tilde{u})^2_{x+\Delta x} = 0 \\ \frac{\partial \mathscr{L}}{\partial C} &= -2\tilde{u}(x) + 2C + \lambda = 0 \\ \frac{\partial \mathscr{L}}{\partial D} &= -2u'(x)(u' + \tilde{u})_{x+\Delta x} + 2B(u' + \tilde{u})^2_{x+\Delta x} + \lambda(u' + \tilde{u})^2_{x+\Delta x} = 0 \end{aligned} \tag{3.5}$$

This gives the extremal values of the coefficients. The stochastic estimates of $\tilde{u}$ and $u'$ can now be found to be:

$$\tilde{u}_E(x) = \frac{1}{2}\left[\frac{\langle \tilde{u}_x(\tilde{u}+u')_{x+\Delta x}\rangle - \langle u'_x(\tilde{u}+u')_{x+\Delta x}\rangle}{\langle(\tilde{u}+u')_{x+\Delta x}(\tilde{u}+u')_{x+\Delta x}\rangle}\right](\tilde{u}+u')_{x+\Delta x} + \frac{1}{2}(\tilde{u}+u')_x \quad (3.6)$$

$$u'_E(x) = -\frac{1}{2}\left[\frac{\langle \tilde{u}_x(\tilde{u}+u')_{x+\Delta x}\rangle - \langle u'_x(\tilde{u}+u')_{x+\Delta x}\rangle}{\langle(\tilde{u}+u')_{x+\Delta x}(\tilde{u}+u')_{x+\Delta x}\rangle}\right](\tilde{u}+u')_{x+\Delta x} + \frac{1}{2}(\tilde{u}+u')_x \quad (3.7)$$

Neglecting cross-correlations and assuming that $\Delta x$ is significantly larger than the longitudinal integral scale, these estimates become:

$$\tilde{u}_E(x) = \frac{1}{2}\left[\frac{\langle(\tilde{u}+u')_x(\tilde{u}+u')_{x+\Delta x}\rangle}{\langle(\tilde{u}+u')_{x+\Delta x}(\tilde{u}+u')_{x+\Delta x}\rangle}\right](\tilde{u}+u')_{x+\Delta x} + \frac{1}{2}(\tilde{u}+u')_x \quad (3.8)$$

and

$$u'_E(x) = -\frac{1}{2}\left[\frac{\langle(\tilde{u}+u')_x(\tilde{u}+u')_{x+\Delta x}\rangle}{\langle(\tilde{u}+u')_{x+\Delta x}(\tilde{u}+u')_{x+\Delta x}\rangle}\right](\tilde{u}+u')_{x+\Delta x} + \frac{1}{2}(\tilde{u}+u')_x\ . \quad (3.9)$$

This estimate of $\tilde{u}$ and $u'$ differs from conventional stochastic estimates in so far as it estimates both $\tilde{u}_E$ and $u'_E$ while constraining their sum to equal $\tilde{u}+u'$. Separate unconstrained stochastic estimates for $\tilde{u}_E$ and $u'_E$ would not necessarily satisfy this decomposition criterion.

## 3.2 Application to planar velocity fields (as measured by MTV, PIV)

Using the knowledge that turbulent variables are completely uncorrelated over large displacements, it is possible to formulate a stochastic estimate of the turbulent and

cyclic components of velocity. This estimate yields the following equations to compute turbulent and cyclic velocity components, which are re-expressions of equations 3.7 and 3.8:

$$\tilde{u}_E(x,t) = \frac{1}{2}\frac{R_{uu,x}(\Delta x)}{R_{uu,x+\Delta x}(0)}[u(x+\Delta x,t) - \langle u(x+\Delta x)\rangle] + \frac{1}{2}[u(x,t) - \langle u(x)\rangle] \quad (3.10)$$

$$u'_E(x,t) = -\frac{1}{2}\frac{R_{uu,x}(\Delta x)}{R_{uu,x+\Delta x}(0)}[u(x+\Delta x,t) - \langle u(x+\Delta x)\rangle] + \frac{1}{2}[u(x,t) - \langle u(x)\rangle] \quad (3.11)$$

where $R_{uu,x}(\Delta x)$ is the two-point correlation tensor,

$$\left\langle \Big[u\,(x,t) - \langle u\,(x)\rangle\Big]\Big[u(x+\Delta x,t) - \langle u(x+\Delta x)\rangle\Big] \right\rangle,$$

and $R_{uu,\Delta x}(0)$ is the single-point correlation tensor

$$\left\langle \Big[u\,(x+\Delta x,t) - \langle u\,(x+\Delta x)\rangle\Big]\Big[u(x+\Delta x,t) - \langle u(x+\Delta x)\rangle\Big] \right\rangle.$$

The time variable, $t$, can be used interchangeably with the cycle number at a given crank angle. The displacement, $\Delta x$, can be either a positive or negative value and is similar to a forward or backward difference in discrete differentiation. One can also form a central difference, as the average of the forward and backward differences, in which case

$$\begin{aligned} u'_E(x,t) = &-\frac{1}{2}\frac{R_{uu,x}(\Delta x)}{R_{uu,x+\Delta x}(0)}[u(x+\Delta x,t) - \langle u(x+\Delta x)\rangle] \\ &-\frac{1}{2}\frac{R_{uu,x}(-\Delta x)}{R_{uu,x-\Delta x}(0)}[u(x-\Delta x,t) - \langle u(x-\Delta x)\rangle] \\ &+\frac{1}{2}[u(x,t) - \langle u(x)\rangle]. \end{aligned} \quad (3.12)$$

This central averaging method was also used to calculate $\tilde{u}$. When the turbulent and cyclic velocity components were calculated at points along the edge of the grid,where central averaging is not possible, either a backward or forward method

was used. This method has been applied to planar velocity field data measured using MTV. Software was written, originally in MATLAB, that can input MTV output data in ASCII tabular form and perform the stochastic decomposition. This decomposition was very slow to carry out with these data sets because MATLAB is not a compiled language and because of the processor speed available at the time. For this reason the code was rewritten in C++[1], which along with the increase in available computing power, resulted in run times sixty times faster, or less than thirty seconds on an 800 MHz processor.

MTV data is written as ASCII text in a tabular format. Columns exist for $x$ position, $y$ position, $u$ velocity, $v$ velocity, time, etc. There is also a column of 'interesting point' numbers which uniquely identify each point in a frame, so that corresponding points in different frames can be identified as corresponding. These 'interesting point' numbers are used by the decomposition program to index the data, and locate the surrounding points to make cross-correlations.

For some MTV experimental data sets, the shape of the field of data was unsuitable for calculating correlations. Preprocessing was required to extract a rectangular field of data from these data sets.

[1]Compiled with GNU C++

# Chapter 4

# Results and Discussion

## 4.1 Qualification – effect of filter size

The displacement distance, or filter size, $\Delta x$, is chosen to distinguish between turbulence and cycle-to-cycle variation in this decomposition. Ideally, correlation length scales for turbulence would be much smaller than those for cyclic unsteadiness making separation of the two components straightforward. Therefore if the displacement $\Delta x$ were chosen to be greater than the correlation length-scale of turbulence, but less than that of cyclic unsteadiness, then a displacement of $2\Delta x$ would also be greater than that of the turbulence correlation length-scale. If it were also less than that of the cyclic unsteadiness one would expect estimates of turbulent and cycle-to-cycle unsteadiness to be similar for displacements $\Delta x$ and $2\Delta x$. To assess this hypothesis, the decomposition was run on sets of data from the Ford 4.6 L engine at 90, 180, and 270 CAD using two different filter sizes. The resulting velocity fields were then averaged to yield a cyclic intensity, defined as

$$\text{Cyclic Intensity}(x,y) = \frac{1}{2}\left\langle \tilde{u}_E(x,y)\tilde{u}_E(x,y) + \tilde{v}_E(x,y)\tilde{v}_E(x,y)\right\rangle \tag{4.1}$$

and a turbulent kinetic energy, defined as

$$\text{Turbulent Kinetic Energy}(x,y) = \frac{1}{2}\left\langle u'_E(x,y)u'_E(x,y) + v'_E(x,y)v'_E(x,y)\right\rangle . \tag{4.2}$$

Tables 4.1 - 4.4 show that as the filter size doubles the increase in turbulent kinetic energy and decrease in cyclic intensity do not account for each other. Consequently, the turbulent and cyclic variation velocities are not correlated over completely different scales, but over scales that overlap, and the decomposition is not unique but appears to depend on the spatial displacement chosen. This is consistent with the expectation that an increase in the filter size would lump more large-scale fluctuation in with the small- scale fluctuation. Therefore, it is more appropriate to consider the decomposition of these velocity fields into fine-scale turbulence and large-scale fluctuations, many of which are cycle-to-cycle variations, but some of which are large-scale turbulence.

In a study by Witze [9] in engines of similar dimensions, he found that from 0 to 270 CAD, the integral length scale of turbulence varied between 1 mm and 7 mm depending on crank angle and location within the cylinder. The standard filter

Table 4.1: Effect of filter size on decomposition of Ford 4.6 L engine data, 90 CAD, 600 rpm, decomposition of 490 cycles.

| | Displacement | | Turbulent Kinetic | Cyclic Intensity |
|---|---|---|---|---|
| Filter | $\Delta x$ (cm) | $\Delta y$ (cm) | Energy ($cm^2/s^2$) | ($cm^2/s^2$) |
| Standard | 0.377879 | 0.392267 | 20761 | 45935 |
| Double | 0.769171 | 0.78172 | 24749 | 32656 |
| Change | +103.55% | +99.28% | +19.21% | -28.91% |

Table 4.2: Effect of filter size on decomposition of Ford 4.6 L engine data, 90 CAD, excitation at 300 Hz, 600 rpm, decomposition of 502 cycles.

| | Displacement | | Turbulent Kinetic | Cyclic Intensity |
|---|---|---|---|---|
| Filter | $\Delta x$ (cm) | $\Delta y$ (cm) | Energy ($cm^2/s^2$) | ($cm^2/s^2$) |
| Standard | 0.375071 | 0.385734 | 15548 | 39731 |
| Double | 0.771965 | 0.769683 | 20398 | 28259 |
| Change | +105.82% | +99.54% | +31.19% | -28.87% |

Table 4.3: Effect of filter size on decomposition of Ford 4.6 L engine data, 180 CAD, 600 rpm, decomposition of 504 cycles.

| | Displacement | | Turbulent Kinetic | Cyclic Intensity |
|---|---|---|---|---|
| Filter | $\Delta x$ (cm) | $\Delta y$ (cm) | Energy ($cm^2/s^2$) | ($cm^2/s^2$) |
| Standard | 0.357076 | 0.394531 | 3617.9 | 13594 |
| Double | 0.728985 | 0.793812 | 5306.7 | 9947.5 |
| Change | +104.15% | +101.20% | +46.68% | -26.82% |

Table 4.4: Effect of filter size on decomposition of Ford 4.6 L engine data, 270 CAD, 600 rpm, decomposition of 499 cycles.

| | Displacement | | Turbulent Kinetic | Cyclic Intensity |
|---|---|---|---|---|
| Filter | $\Delta x$ (cm) | $\Delta y$ (cm) | Energy ($cm^2/s^2$) | ($cm^2/s^2$) |
| Standard | 0.370316 | 0.382976 | 2479.5 | 9455.5 |
| Double | 0.752045 | 0.766314 | 3307.3 | 7593.5 |
| Change | +103.08% | +100.09% | +33.39% | -19.69% |

size in our decomposition of data from the Ford engine sets $\Delta x$ and $\Delta y$ slightly less than 4 mm, while the double filter size sets $\Delta x$ and $\Delta y$ slightly less than 8 mm. The decomposition of data from the MSU engine uses a filter with $\Delta x \approx 5$ mm and $\Delta y \approx 3$ mm. The choice of filter size seems appropriate. It therefore appears that large-scale turbulence and cycle-to-cycle variation in these engine cylinder flows have overlapping correlations at large (4 mm) displacements and that this decomposition is at best an estimate in these flows.

## 4.2 Method of presenting decomposed data

On the following pages, several figures show graphical examples of stochastically decomposed flowfields. Figure 4.1 shows the plane of view used in both engines from a top-down view. Figures 4.2 through 4.5 show the field of view in the cylinder of

each engine for each crank angle used. The decomposed flowfield from one engine cycle in the Ford 4.6 L engine at 90 CAD is shown in Figure 4.6. This figure shows the instantaneous, or total velocity, as well as the three components that make up the total velocity at this particular cycle. The plot labeled "Total Velocity" in this figure shows the in-cylinder velocity vectors as measured using MTV at a single instant in time. The plot labeled "Average Velocity" shows the mean velocity vectors calculated from the ensemble of 490 engine cycles at the same crank angle. Also shown are the turbulent components and the cyclic components of the velocity for this particular instant in time. It can be observed that at each data-point the total velocity is the vector sum of the turbulent, cyclic, and average vectors.

### 4.2.1 Edge effects

At edges of velocity fields, where there are no neighboring points with which correlations can be made, it is not possible to make stochastic estimates of $\tilde{u}_E$ and $u'_E$, so they are arbitrarily set to zero. This can be seen in Figure 4.7, which shows a sample flowfield from the Ford 4.6 L engine at the 90 CAD with excitation at 300 Hz. The two vectors along the left side of the total velocity plot, near the top, are not equal to their complementary vectors in the average velocity plot. However, there is no cyclic or turbulent component at this location to account for the difference. An alternative treatment would be to not present any decomposed data at such locations.

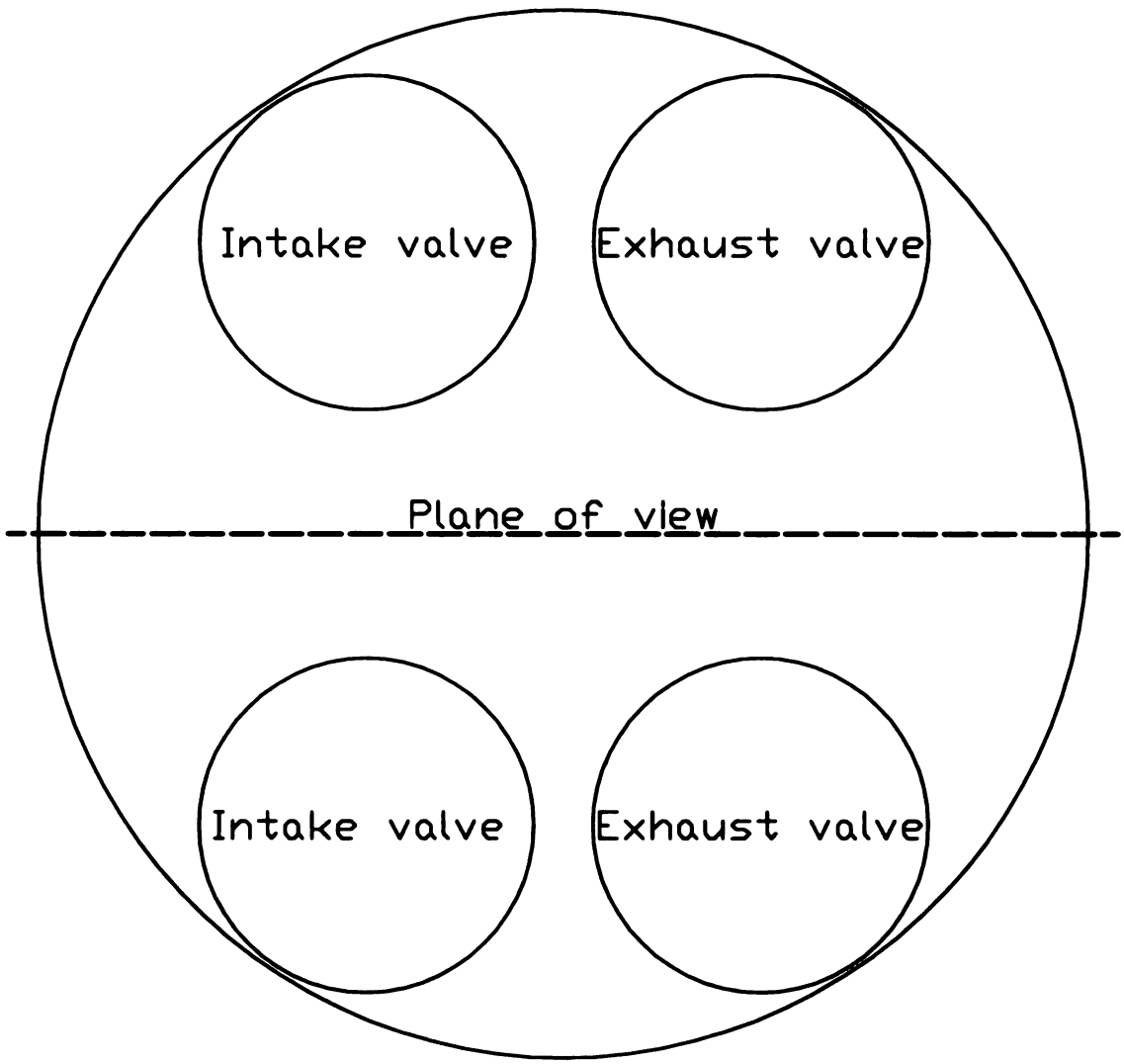


Figure 4.1: Top-down representation of plane of view in cylinder of engine

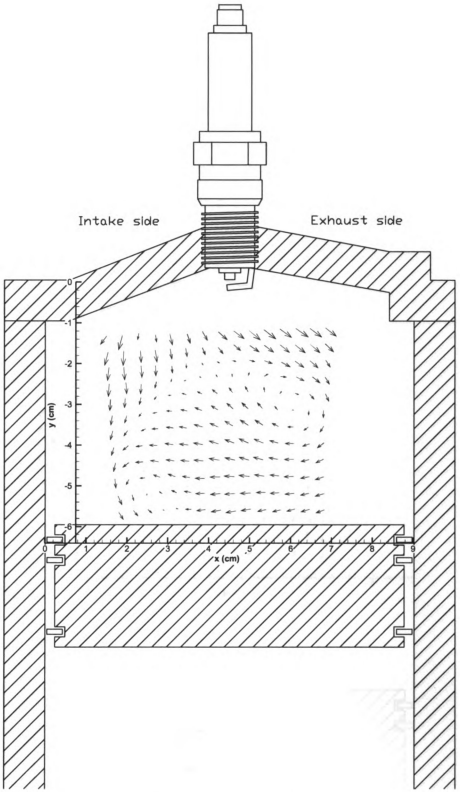


Figure 4.2: Representation of field of view relative to cylinder of Ford 4.6 L engine at 90 (and 270) CAD

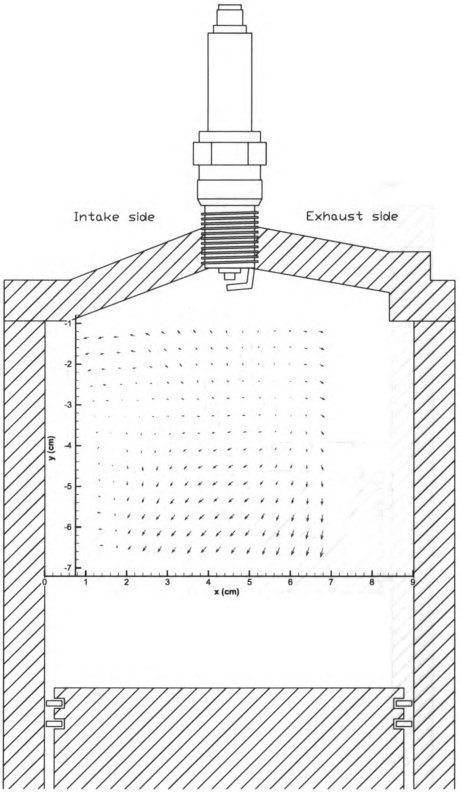


Figure 4.3: Representation of field of view relative to cylinder of Ford 4.6 L engine at 180 CAD

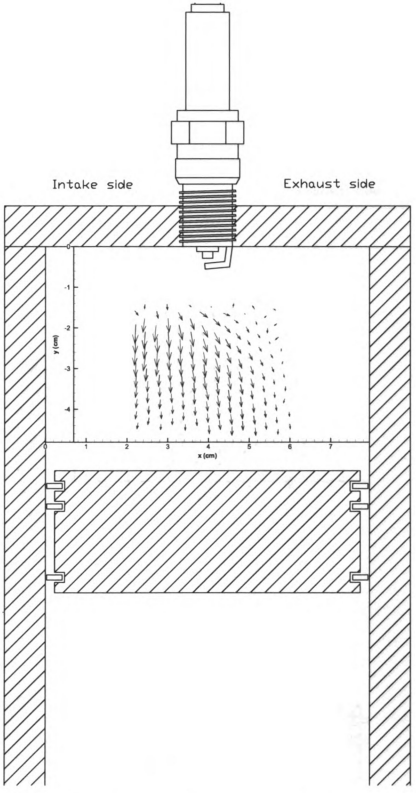


Figure 4.4: Representation of field of view relative to cylinder of MSU engine at 90 (and 270) CAD

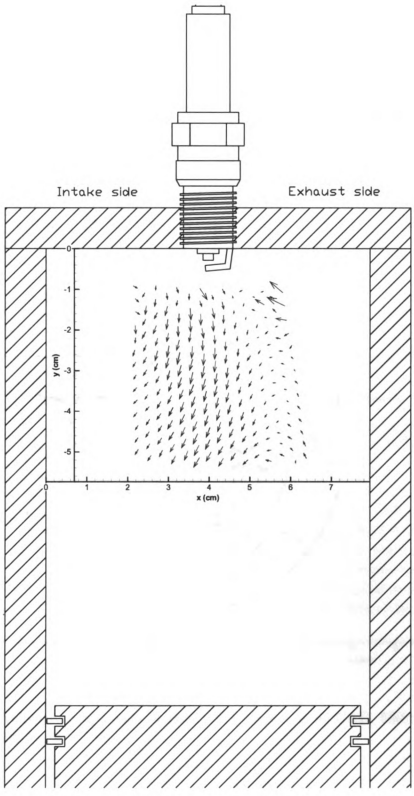


Figure 4.5: Representation of field of view relative to cylinder of MSU engine at 180 CAD

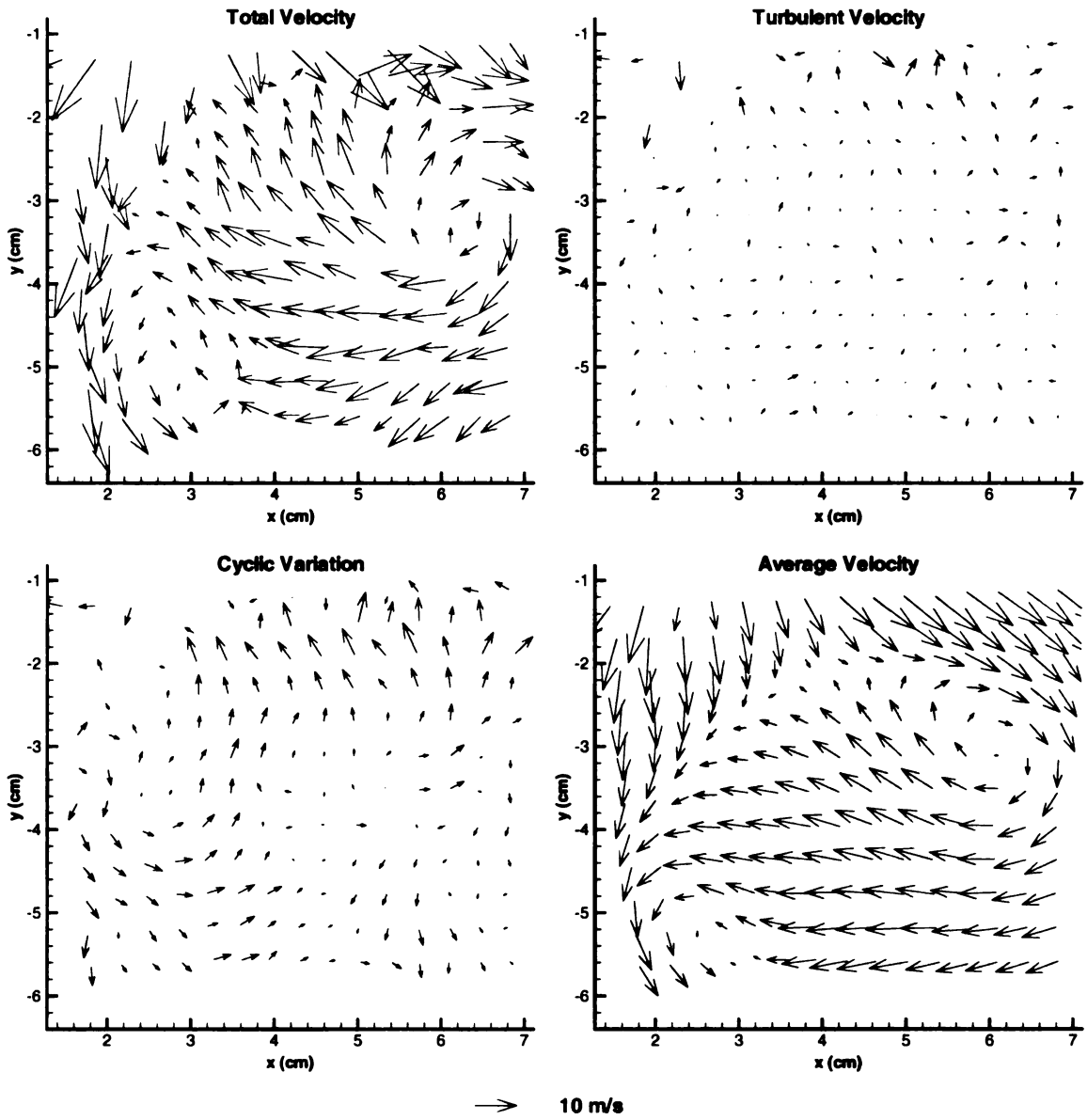


Figure 4.6: Velocity components of Ford 4.6 L engine at 90 CAD, 600 rpm, decomposition of 490 cycles

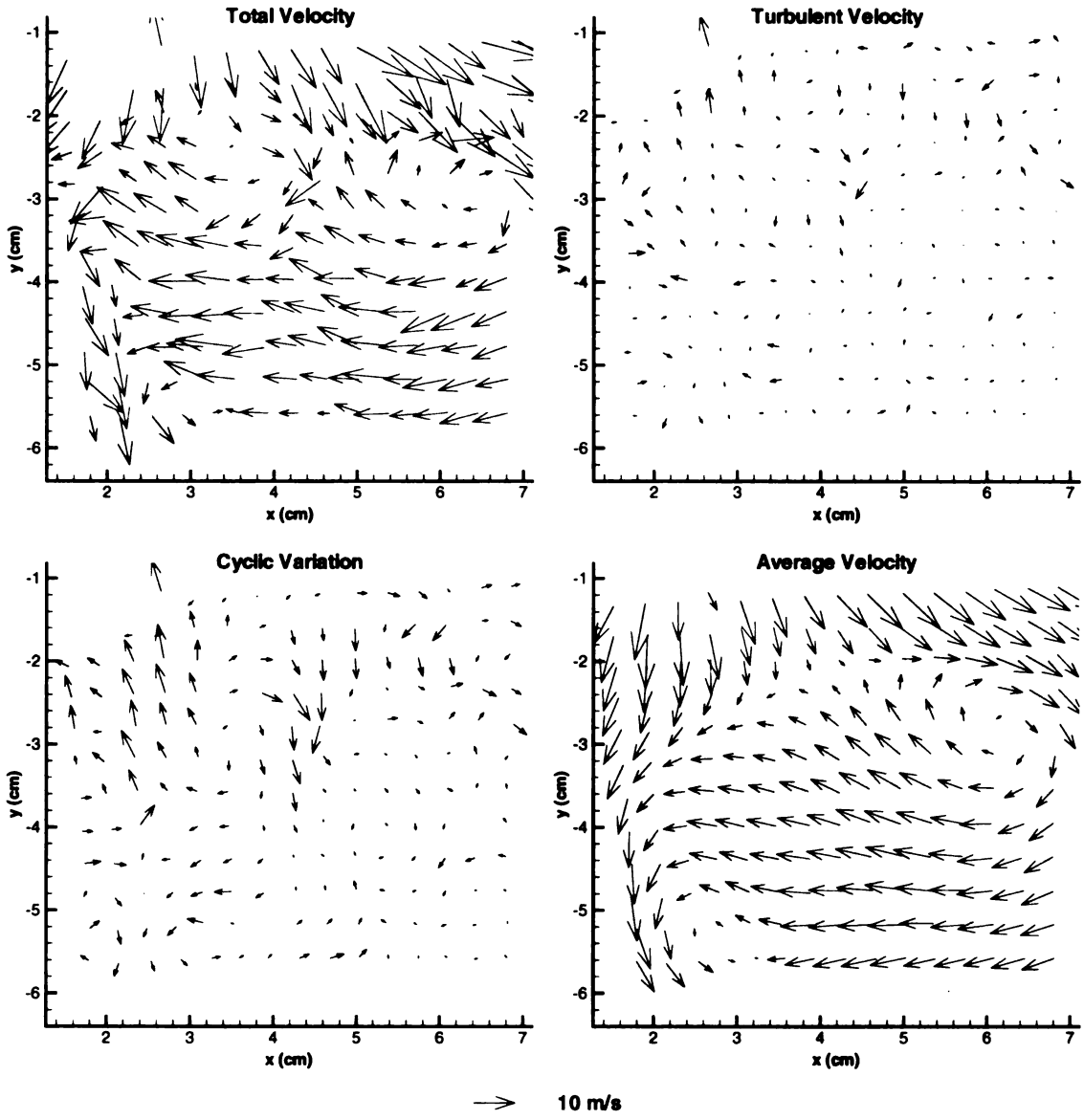


Figure 4.7: Velocity components of Ford 4.6 L engine at 90 CAD, excitation at 300 Hz, 600 rpm, decomposition of 502 cycles

## 4.3 Decomposition of excited in-cylinder flow

### 4.3.1 Ford 4.6 L engine turbulent and cyclic kinetic energy

Planar velocity fields measured in a motored Ford 4.6 liter engine at 600 rpm were decomposed using the stochastic estimations technique and a filter length of $\Delta x \approx$ 0.4 cm. Table 4.5 shows the effects of excitation on the fine-scale turbulent kinetic energy, as deduced by this decomposition, at different crank angles. The values shown in this table and similar ones are calculated as a percentage of the turbulent kinetic energy at 90 CAD with no excitation. Except at 180 CAD where little change is evident, a slight decrease in fine-scale turbulent kinetic energy appears to result from the presence of excitation, according to this decomposition. The effects of excitation on kinetic energy in cyclic variation is shown in Table 4.6. Again the presence of excitation results in a decrease in large scale turbulent/cyclic variation, although small.

Table 4.5: Effects of excitation on turbulent kinetic energy in Ford 4.6 L engine at 600 rpm.

| Crank Angle | 90° | 180° | 270° |
|---|---|---|---|
| No Excitation | 100% | 17.4% | 11.9% |
| Excitation at 300 Hz | 74.9% | 16.4% | 8.0% |
| Excitation at 400 Hz | 94.3% | 16.8% | 8.0% |

Table 4.6: Effects of excitation on cycle-to-cycle kinetic energy in Ford 4.6 L engine at 600 rpm.

| Crank Angle | 90° | 180° | 270° |
|---|---|---|---|
| No Excitation | 100% | 29.6% | 20.6% |
| Excitation at 300 Hz | 86.5% | 29.3% | 20.0% |
| Excitation at 400 Hz | 91.1% | 29.2% | 18.9% |

The values calculated for the rate of production of fine-scale turbulence in this engine are shown in Table 4.7, where the production rate is defined as:

$$\text{Production Rate} = -u'^2\frac{du}{dx} + -v'^2\frac{dv}{dy} + -u'v'\left(\frac{du}{dy} + \frac{dv}{dx}\right), \tag{4.3}$$

where

$$\frac{di}{dj} = \frac{\frac{(\bar{i}+\bar{i})_{j+\Delta j}-(\bar{i}+\bar{i})}{i_{j+\Delta j}-i} + \frac{(\bar{i}+\bar{i})_{j-\Delta j}-(\bar{i}+\bar{i})}{i_{j-\Delta j}-i}}{2}.$$

These data indicate that the excitation decreases the rate at which new turbulence is created.

Figures 4.8 to 4.11 each show an individual cycle from the decomposition of data at 180 CAD and 270 CAD.

Table 4.7: Effects of excitation on rate of production of fine-scale turbulence in the Ford 4.6 L engine at 600 rpm.

| Crank Angle | 90° | 180° | 270° |
|---|---|---|---|
| No Excitation | 100% | −1.8% | 4.7% |
| Excitation at 300 Hz | 86.9% | −0.2% | 2.3% |
| Excitation at 400 Hz | 54.8% | −0.8% | 2.3% |

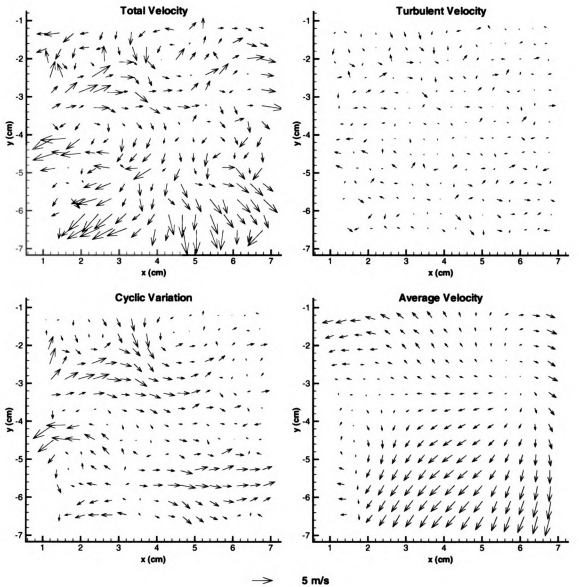


Figure 4.8: Velocity components of Ford 4.6 L engine at 180 CAD, 600 rpm, decomposition of 504 cycles

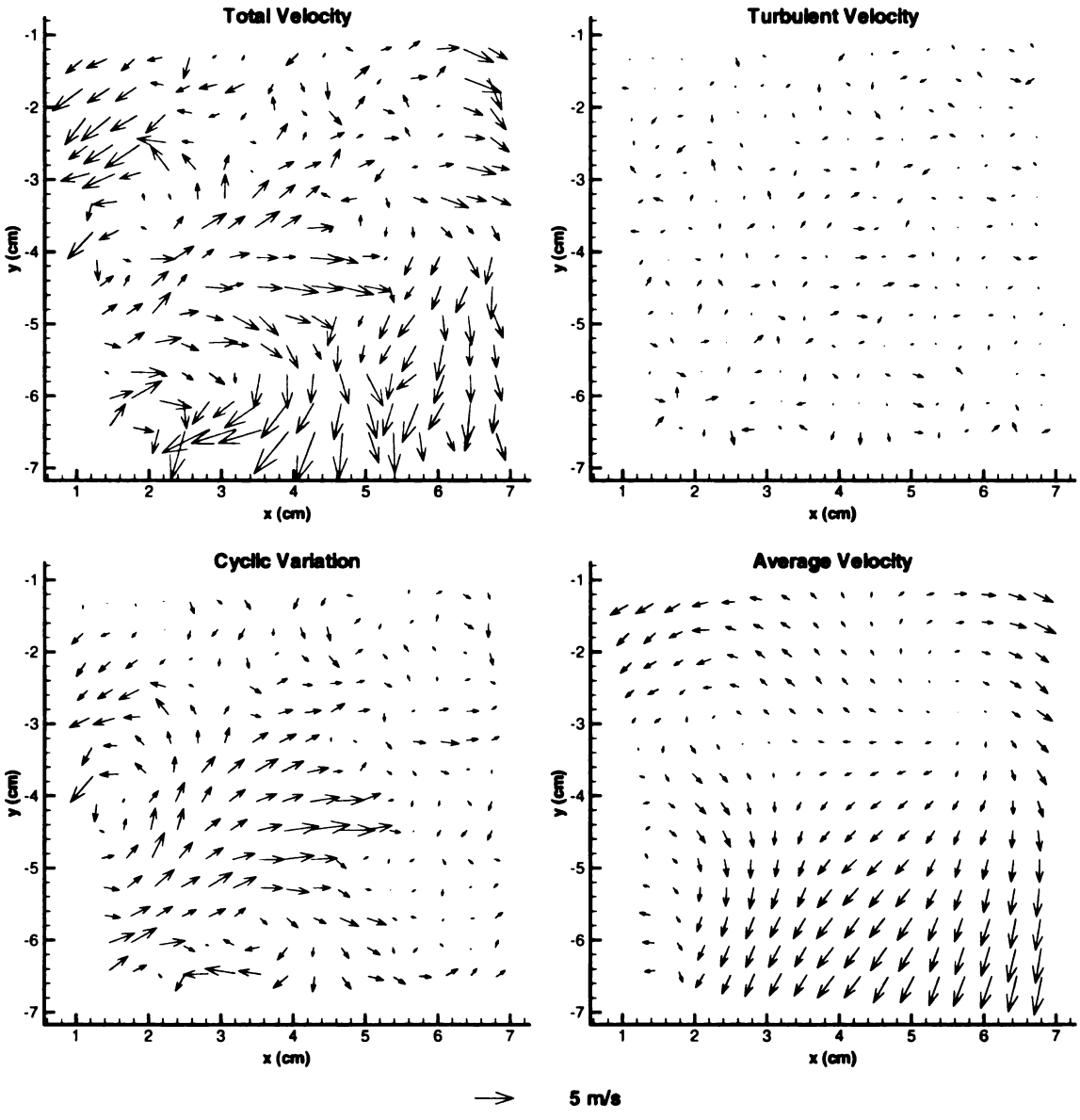


Figure 4.9: Velocity components of Ford 4.6 L engine at 180 CAD, with excitation at 300 Hz, 600 rpm, decomposition of 501 cycles

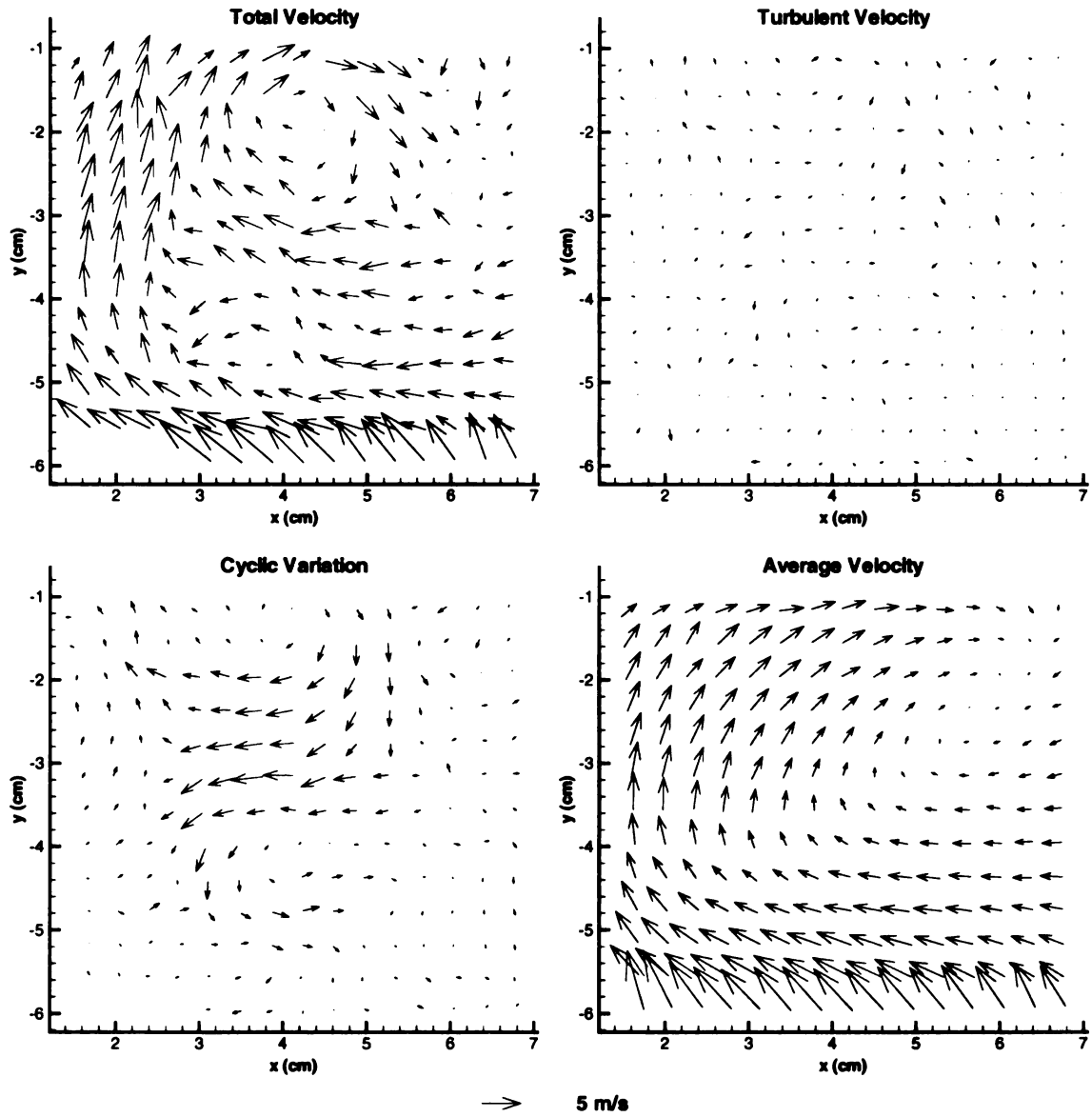


Figure 4.10: Velocity components of Ford 4.6 L engine at 270 CAD, 600 rpm, decomposition of 499 cycles

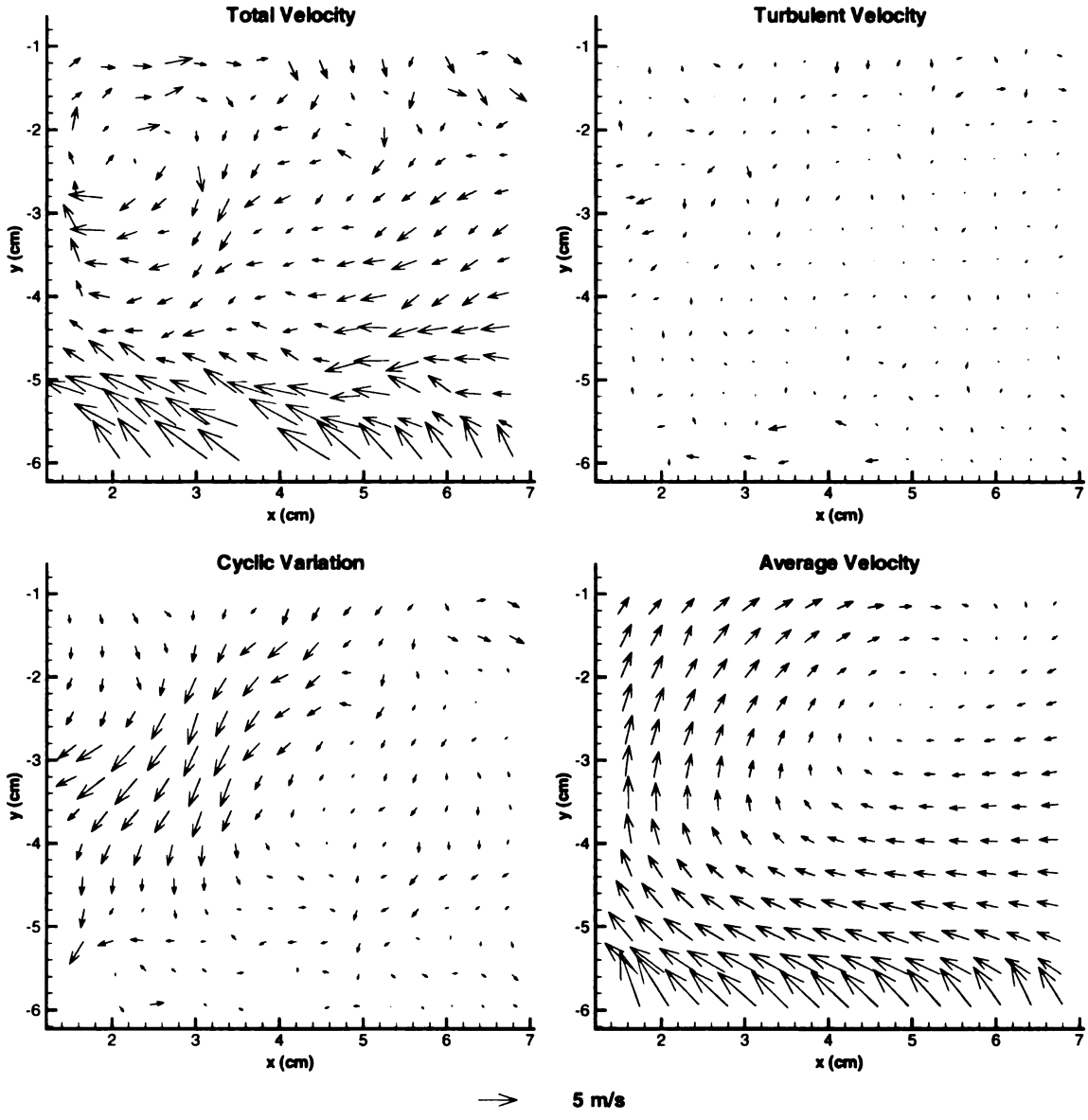


Figure 4.11: Velocity components of Ford 4.6 L engine at 270 CAD, with excitation at 300 Hz, 600 rpm, decomposition of 503 cycles

### 4.3.2 MSU flat-head engine turbulent and cyclic kinetic energy

For this engine, effects of acoustic excitation were investigated only at 270 CAD. Reference data was obtained at 90 CAD and 180 CAD and 270 CAD. Table 4.8 shows the effects of excitation on turbulent kinetic energy, as deduced by this decomposition, at 270 CAD for the MSU flat-head engine. This table shows that excitation decreases the turbulent kinetic energy, with certain frequencies less effective than others. Table 4.9 shows the effects of excitation on kinetic energy in cyclic variation at 270 CAD for the MSU flat-head engine. The excitation causes a much greater decrease in cyclic variation, relative to both the reference value at 90 CAD and at 270 CAD, than was seen for the Ford 4.6 L engine. The greater effect of the excitation could be caused by several things: higher intake velocity resulting from the increase in rpm, intake geometry, or because the excitation is more effective at the higher frequencies used by Fedewa. Table 4.10 shows the turbulent production rate values calculated for this engine. Just as in the Ford 4.6 L engine, the MSU flat-head engine produces less

Table 4.8: Effects of excitation on turbulent kinetic energy in MSU flat-head engine at 1500 rpm.

| Crank Angle | 90° | 180° | 270° |
|---|---|---|---|
| No Excitation | 100% | 11.4% | 5.1% |
| Excitation at 1500 Hz | | | 3.3% |
| Excitation at 1600 Hz | | | 4.2% |
| Excitation at 1700 Hz | | | 4.2% |
| Excitation at 1800 Hz | | | 2.4% |
| Excitation at 1900 Hz | | | 2.5% |
| Excitation at 2000 Hz | | | 2.6% |
| Excitation at 2100 Hz | | | 2.6% |
| Excitation at 2200 Hz | | | 3.9% |
| Excitation at 2300 Hz | | | 3.9% |
| Excitation at 2400 Hz | | | 2.6% |
| Excitation at 2500 Hz | | | 2.4% |

Table 4.9: Effects of excitation on cycle-to-cycle kinetic energy in MSU flat-head engine at 1500 rpm.

| Crank Angle | 90° | 180° | 270° |
|---|---|---|---|
| No Excitation | 100% | 25.9% | 13.3% |
| Excitation at 1500 Hz | | | 5.8% |
| Excitation at 1600 Hz | | | 7.0% |
| Excitation at 1700 Hz | | | 10.6% |
| Excitation at 1800 Hz | | | 6.3% |
| Excitation at 1900 Hz | | | 5.5% |
| Excitation at 2000 Hz | | | 5.6% |
| Excitation at 2100 Hz | | | 5.6% |
| Excitation at 2200 Hz | | | 10.9% |
| Excitation at 2300 Hz | | | 10.9% |
| Excitation at 2400 Hz | | | 5.7% |
| Excitation at 2500 Hz | | | 5.3% |

Table 4.10: Effects of excitation on production rate in MSU flat-head engine at 1500 rpm.

| Crank Angle | 90° | 180° | 270° |
|---|---|---|---|
| No Excitation | 100% | −2.2% | −1.4% |
| Excitation at 1500 Hz | | | −0.5% |
| Excitation at 1600 Hz | | | −0.6% |
| Excitation at 1700 Hz | | | −0.5% |
| Excitation at 1800 Hz | | | −0.3% |
| Excitation at 1900 Hz | | | −0.2% |
| Excitation at 2000 Hz | | | −0.4% |
| Excitation at 2100 Hz | | | −0.4% |
| Excitation at 2200 Hz | | | −0.7% |
| Excitation at 2300 Hz | | | −0.7% |
| Excitation at 2400 Hz | | | −0.4% |
| Excitation at 2500 Hz | | | −0.4% |

turbulence when excitation is present.

An example engine cycle from the reference data, taken at 90 CAD with no excitation is shown in Figure 4.12 and a cycle from data taken at 180 CAD with no excitation is shown in Figure 4.13.

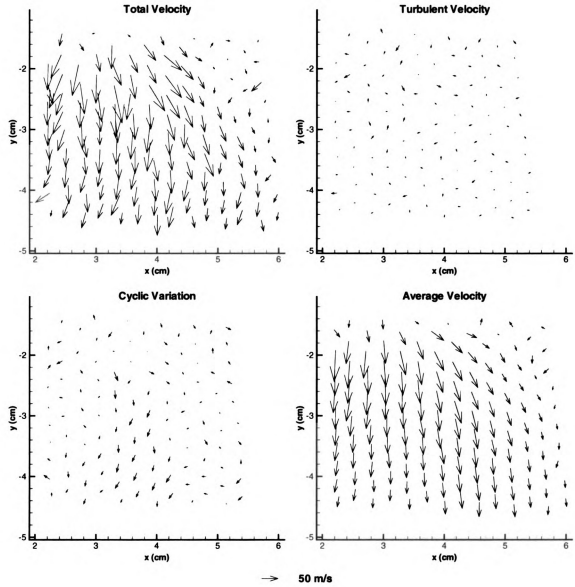


Figure 4.12: Velocity components of MSU flat-head engine at 90 CAD, 1500 rpm, decomposition of 500 cycles

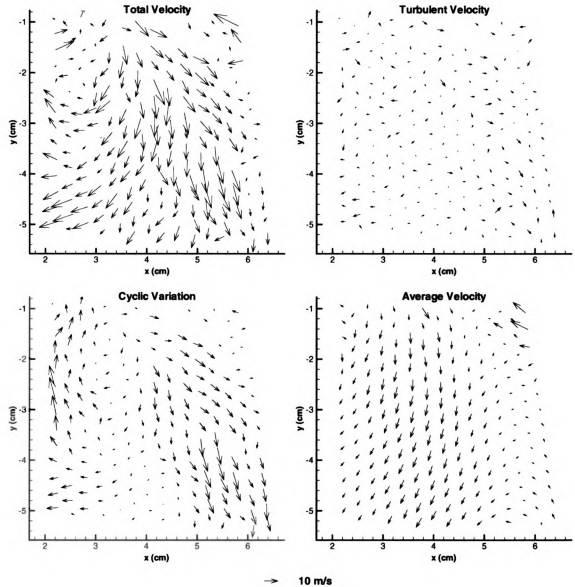


Figure 4.13: Velocity components of MSU flat-head engine at 180 CAD, 1500 rpm, decomposition of 500 cycles

The flowfield at 270 CAD with no excitation is shown in Figure 4.14, which can be compared to flowfields with excitation at 1900 Hz (Figure 4.15) and 2200 Hz (Figure 4.16).

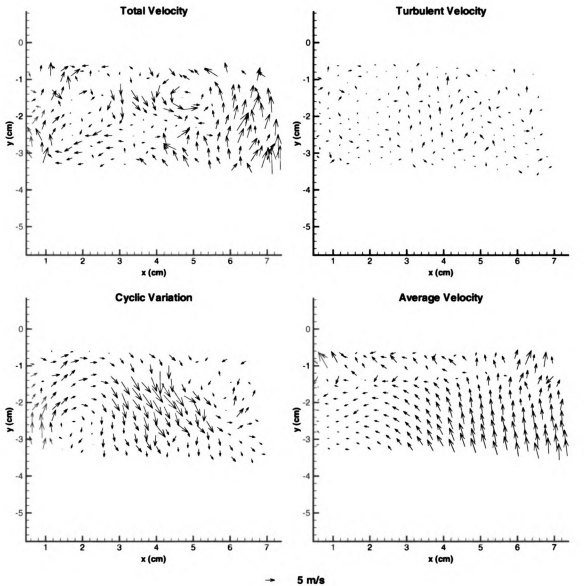


Figure 4.14: Velocity components of MSU flat-head engine at 270 CAD, 1500 rpm, decomposition of 500 cycles

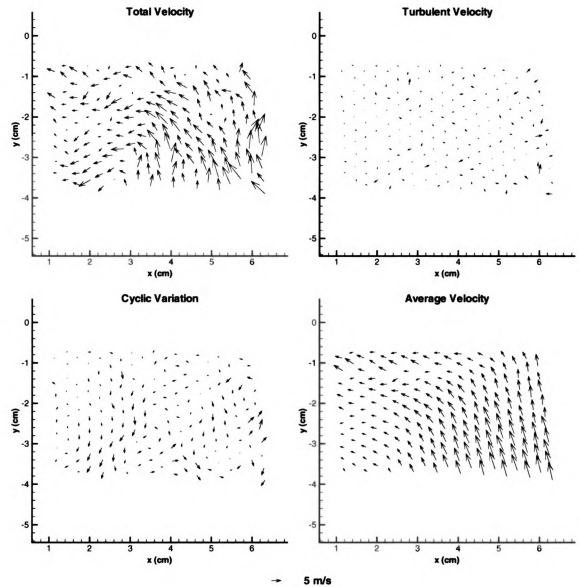


Figure 4.15: Velocity components of MSU flat-head engine at 270 CAD, with excitation at 1900 Hz, 1500 rpm, decomposition of 500 cycles

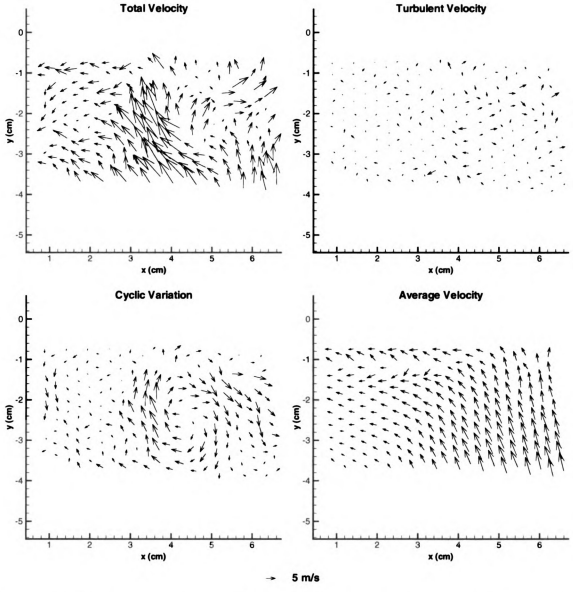


Figure 4.16: Velocity components of MSU flat-head engine at 270 CAD, with excitation at 2200 Hz, 1500 rpm, decomposition of 500 cycles

# Chapter 5

# Conclusions and Recommendations

## 5.1 Conclusions

Software was created to apply a stochastic estimation technique to decompose planar engine-cylinder velocity fields into its three components, namely turbulence, cyclic variation, and mean flow. This software was written specifically to post-process data obtained using Molecular Tagging Velocimetry. Data acquired by Goh and by Fedewa in the course of their research was analyzed to test this decomposition method. The data from each study came from different engines. Goh used a custom engine based on a 4-valve 4.6 L V8 prototype engine, and Fedewa used a Hatz 1D81Z single cylinder diesel engine. The conclusions of this study are:

1. Decomposition by stochastic estimation is a potentially useful tool both for visualizing components of engine velocity fields in individual realizations and for estimating statistics of components of decomposed velocity fields.

2. The decomposition is an estimate of the turbulent and cyclic variation velocity fields, but, in these flows their spatial correlations overlap and estimates depend somewhat on the chosen correlation displacement length $\Delta x$, much like high-pass filters depend on their cut-off value.

3. Although the turbulent and cyclic variation statistics should not be claimed to be those of the true turbulent and cyclic variation fields, the trends in their values, particularly in experiments involving excitation, are of considerable interest.

4. The sensitivity of the decomposition to the choice of $\Delta x$ suggest that the 'turbulent' component is really a 'small-scale turbulent' part and the 'cyclic variation' component may actually be a sum of large-scale turbulence and cycle-to-cycle variation.

5. Visualizations of MTV measurements of engine flows, using these decompositions, can be viewed cycle after cycle on a computer, and are very instructive as to the degree to which large-scale motions can change completely from one cycle to another.

## 5.2 Recommendations

An interesting topic for further study of this decomposition method would be to attempt better validation of it, in non-stationary flows in which turbulence and unsteadiness have much less overlap in spatial correlations. Another approach might be to explore flows which are purposefully made non-stationary. For example, one could process data from an engine with two intake valves, where one of the valves is kept closed during intake for a small percentage of the total number of cycles (i.e. 5%). One would expect to see a considerable amount of cyclic variation while this valve is closed, particularly at 90 CAD.

# Appendices

# Appendix A Integral scale of length and trend in correlations

Since the decomposition scheme is based on the use of correlation functions, and the expectation that turbulent quantities separated by more than roughly an integral scale will be uncorrelated, is is useful to show the behavior of correlations in these in-cylinder flows. In Figures A.1 to A.4 the turbulent correlation functions $Ruu(x)$ and $Ruu(y)$ are shown and each approaches zero after, typically, two or three displacements, $\Delta x$. However, there is considerable "oscillation" about the displacement axis at larger displacements, which would appear as noise or uncertainty in the decomposition. It is not clear if these correlation functions would converge more smoothly to zero at large multiples of $\Delta x$ if more data had been sampled.

The integral scale is defined as the distance along the displacement axis, multiplied by a height of one unit, that is equal to the area between the correlation curve and the displacement axis. From inspection of the correlation functions in Figure A.1, the integral scale would appear to be about one or two displacements, $\Delta x$, which is consistent with the assumptions of the decomposition method.

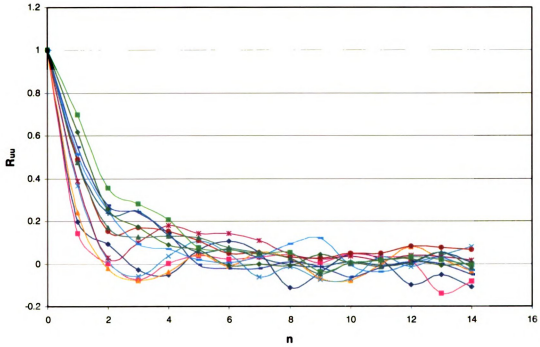


Figure A.1: Trend in $R_{uu,x}(n\Delta x)$ as $n$ increases for 4.6 L Ford engine at 90 CAD

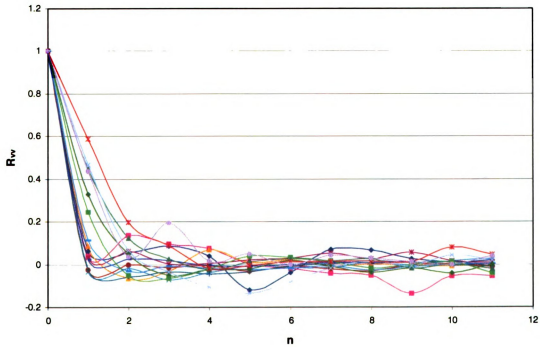


Figure A.2: Trend in $R_{vv,y}(n\Delta y)$ as $n$ increases for 4.6 L Ford engine at 90 CAD

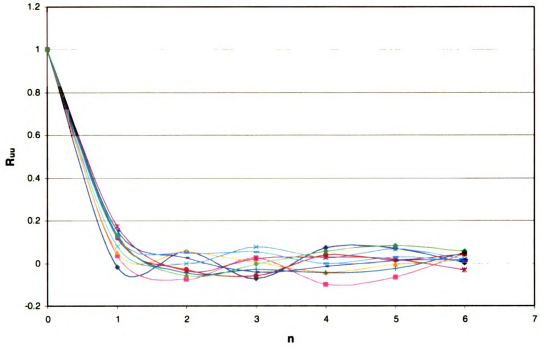


Figure A.3: Trend in $R_{uu,x}(n\Delta x)$ as $n$ increases for MSU engine at 90 CAD

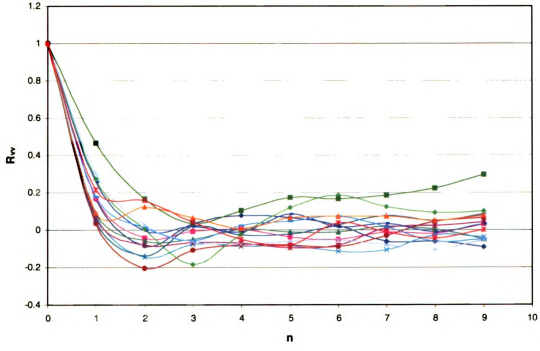


Figure A.4: Trend in $R_{vv,y}(n\Delta y)$ as $n$ increases for MSU engine at 90 CAD

# Appendix B Convergence of average velocities

In order to assure that a sufficient number of cycles were decomposed, the average velocity was tested for convergence. The average velocity data at a point near the center of the flow field was calculated as a function of the number of data sets used.Figures B.1 and B.2 show the ensemble average of $u, v, u^2$, and $v^2$ as the number of cycles included in the decomposition increases. In general, there is little change in the averages provided more than 200 cycles of data are taken, for both mean velocities and turbulence intensities. All decomposed data were based on at least 490 cycles. For the measurements made in MSU engine at 90 CAD, the $v$ and $vv$ averages appear to change monotonically with increasing numbers of realizations. This result is not understood.

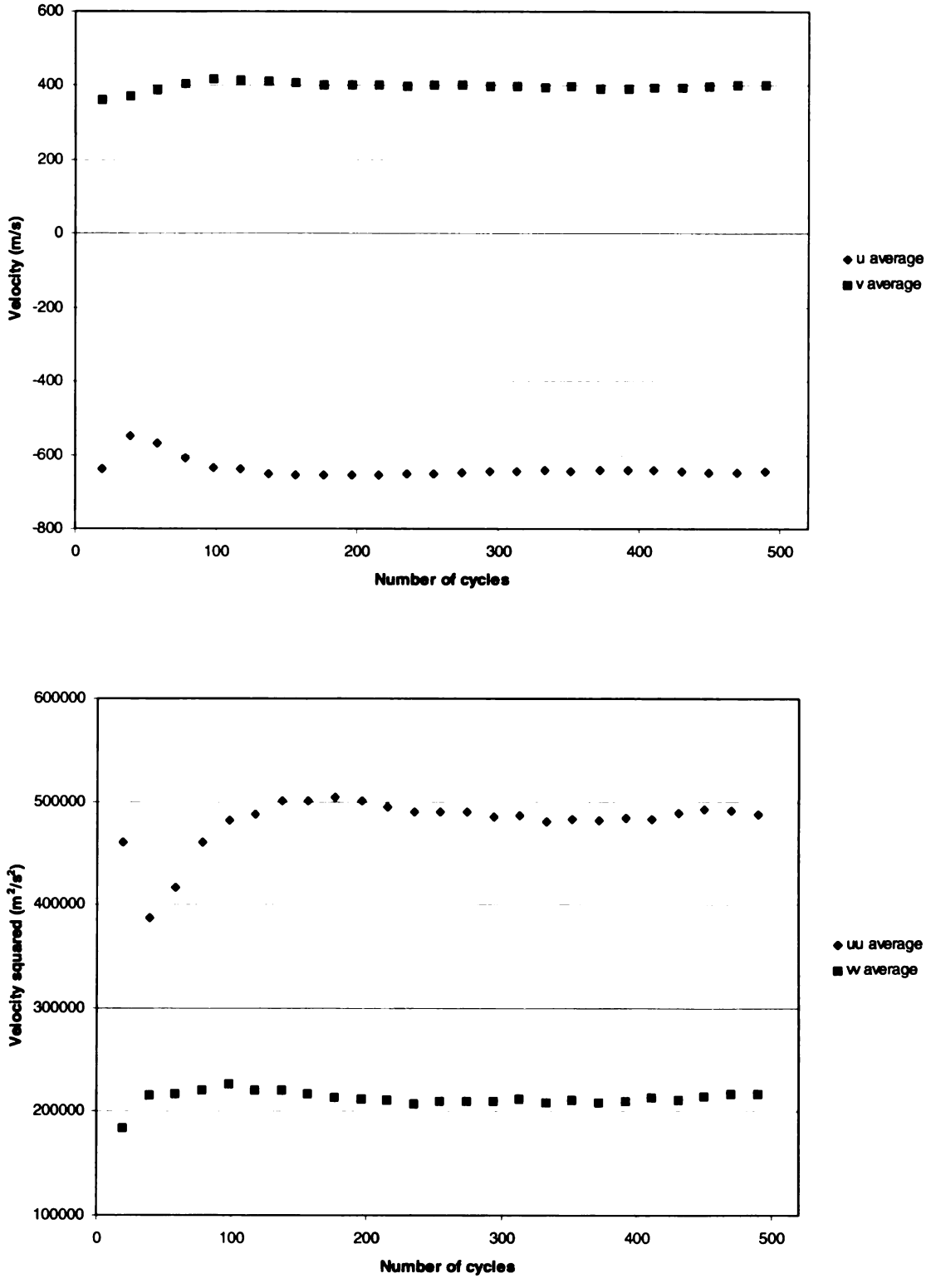


Figure B.1: Convergence of velocities in 4.6 L Ford engine at 90 CAD

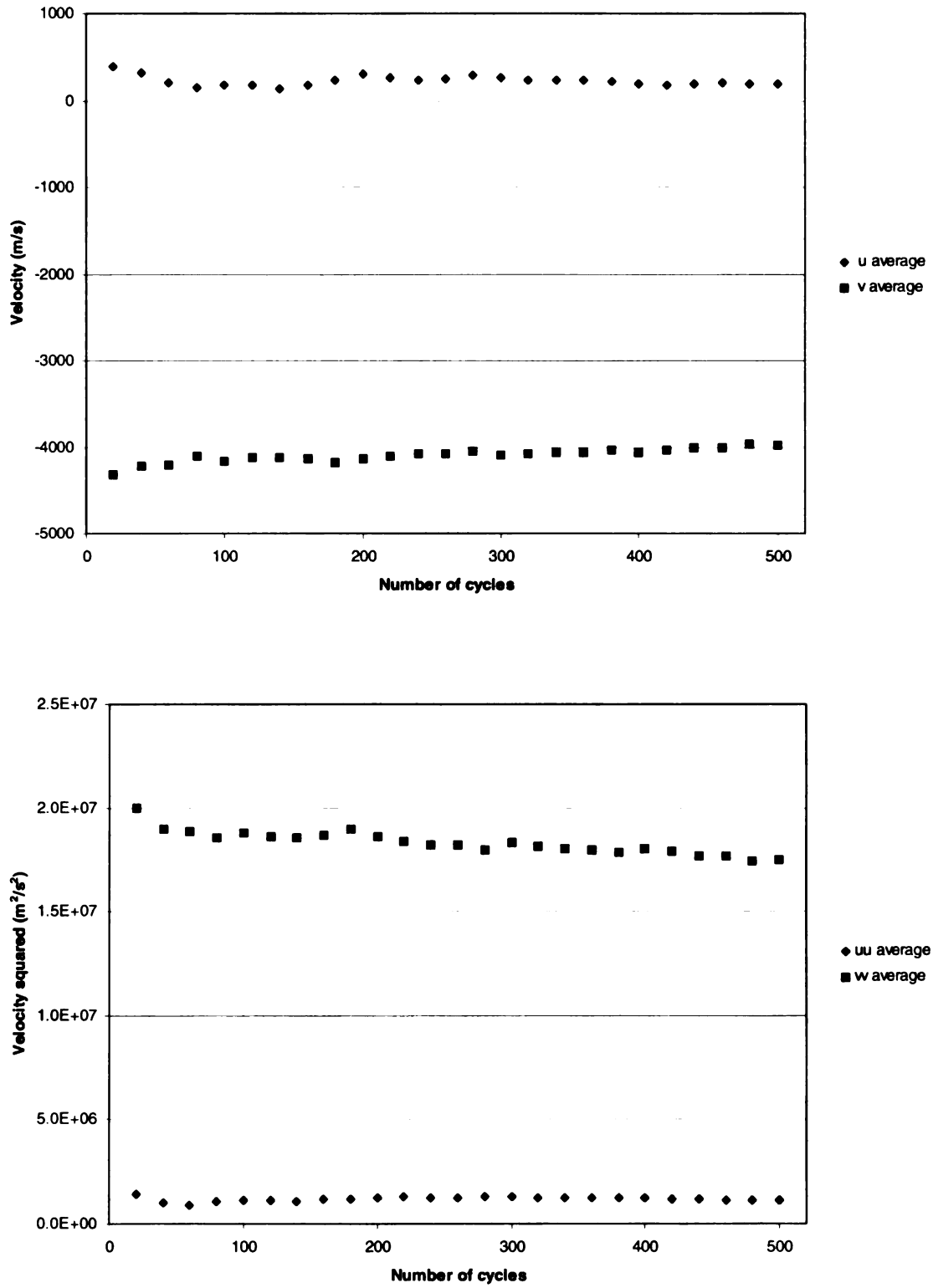


Figure B.2: Convergence of velocities in MSU engine at 90 CAD

# Bibliography


[1] M. J. Hall and F. V. Bracco, "A study of velocities and turbulence intensities measured in firing and motored engines," SAE Paper No. 870453, 1987.

[2] G. J. Brereton and A. Kodal, "An adaptive turbulence filter for decomposition of organized turbulent flows," Phys. Fluids 6, 1775 (1994).

[3] R. J. Adrian and B. G. Jones, M. K. Chung, Y. Hassan, C. K. Nithianandan, and A. T.-C. Tung, "Approximation of turbulent conditional averages by stochastic estimation," Phys Fluids A 1, 992 (1989).

[4] G. J. Brereton, "Stochastical estimation as a statistical tool for approximating turbulent conditional averages," Phys. Fluids A 4, 2046 (1992).

[5] Y. G. Guezennec, "Stochastic estimation of coherent structure in turbulent boundary layers," Phys. Fluids A 1, 1054 (1989).

[6] G. J. Brereton, "Decomposition of non-stationary, non-ergodic turbulence data by stochastic estimation," Phys. Fluids Brief Communication (July 2000).

[7] Goh, A. C. H., "Active flow control for maximizing performance of spark-ignited stratified charge engines," Master's Thesis, Michigan State University, 2001.

[8] Fedewa, A. M., "The effect of active flow control on in cylinder flow and engine performance," Master's Thesis, Michigan State University, 2002.

[9] Witze, P. O., "Measurements of the spatial distribution and engine speed dependence of turbulent air motion in an I.C. Engine," SAE Trans., Vol. 86, Paper No. 770220, pp. 1012-1023, 1977.